

Catalytic Effect on Ionization of Hydrogen

W. Oohara and O. Fukumasa

Graduate School of Science and Engineering, Yamaguchi University, Ube 755-8611, Japan

(Received: 1 September 2008 / Accepted: 8 December 2008)

In a plasma source development of a hydrogen pair-ion plasma consisting of only hydrogen atomic ions, H^+ and H^- , efficient production of the atomic ions is required. Hydrogen positive ions produced in a PIG discharge are supplied to a catalyst. The ions are converted to the atomic ions on the catalyst surface, and an ionic plasma with very low electron density is generated.

Keywords: ionic plasma, catalyst, hydrogen atomic ions

1. Introduction

Pair plasmas consisting of only positive- and negative-charge particles of equal mass have attracted special attention because they maintain space-time symmetry [1–5]. Instead of the electron-positron pair plasmas in high-energy physics and astrophysics [6–8], a fullerene pair-ion plasma, consisting of positive and negative ions of equal mass (C_{60}^+ and C_{60}^-), has been generated and its collective phenomena have been investigated experimentally [9–12]. The response frequency of the pair-ion plasma is limited to a narrow frequency range below 50 kHz because of the massive ions. In order to investigate more extensive physical properties of pair plasmas, particularly wave-propagation characteristics up to higher frequencies, the development of a hydrogen pair-ion plasma source has been started [11], because atomic hydrogen ions are the lightest ions and have high response frequencies to electromagnetic fields. Several difficulties that must be overcome exist in this development, and the most crucial problem is the efficient production of hydrogen negative ions, H^- .

The research and development of negative-ion sources have been extensively performed for more than 20 years in connection with neutral beam injection (NBI) heating for fusion-oriented plasmas [13] and ion guns for the run-up of proton accelerators [14]. The production method of H^- [15] is classified into surface production and volume production [16], and a cesium-seeded multicusp type of ion source is the most successful ion source at present. However, there is the possibility of impurity interdiffusion in that system. Alkali metals, such as Cs, with low evaporation temperatures cannot be used here for the generation of the pair-ion plasma. Our objective is to produce H^- effectively using a catalyst instead of alkali metals.

2. Diffusion-Type Plasma Source

A schematic diagram of the experimental arrangement is illustrated in Fig. 1. The plasma source mainly consists of a hollow Penning ionization gauge (PIG) discharge region and a negative-ion production

part. Two annular cathodes are oppositely located in a cylindrical anode with an inner diameter of 7.5 cm and a length of 15 cm in a uniform magnetic field ($B = 65$ mT), and a tungsten ring filament of 0.5 mm diameter, applied at the same voltage as the cathodes, is set in front of one of the cathodes to supply thermal electrons. The thermal electrons are accelerated in a sheath formed in front of the cathode and injected into the space between the two cathodes, and the accelerated electrons are reflected in the sheath in front of the opposite cathode (anticathode) because the same voltage V_k is applied to both cathodes. Since the electrons are electrostatically confined between the two cathodes along the B -field lines, neutral particles can be efficiently ionized by electron impact, producing positive ions H^+ , H_2^+ , and H_3^+ . The electrons pass transversely across the B -field lines because of the collision and reach the cylindrical anode; thus, a discharge current I_k is observed to flow. In normal operation, the cathodes are typically biased at $V_k \simeq -140$ V (fixed $I_k = 2$ A) with respect to the grounded anode. The back-pressure of the vacuum system is 1×10^{-4} Pa. During operation, a continuous flow of hydrogen is maintained (20 SCCM) and the operating pressure in the source is about 2×10^{-1} Pa.

H^- production is attempted on a cylindrical grid of nickel (Ni), a promising catalyst, which is set in the center of the cylindrical anode and heated by plasma irradiation and particle impact. The Ni grid is 200 mesh, wire diameter of 0.05 mm, open area of 37 %, and opening of 77 μm . The grid is not heated actively by resistive heating and is grounded here ($P_g = 0$ W). The temperature of the grid is about 440 °C. Positive ions and neutral hydrogen inwardly diffuse from the hollow discharge region to the central region through the grid. They come into contact and react with the grid surface in the process of diffusion. The diffused plasma flows downstream and terminates at an end plate ($z = 44$ cm) with a center aperture of 1 mm diameter from the source exit ($z = 0$ cm). An omegatron situated behind the end plate is a chirp-type mass spectrometer [17]. In the omegatron, an rf (radio frequency) electric field is applied in the direc-

author's e-mail: oohara@yamaguchi-u.ac.jp

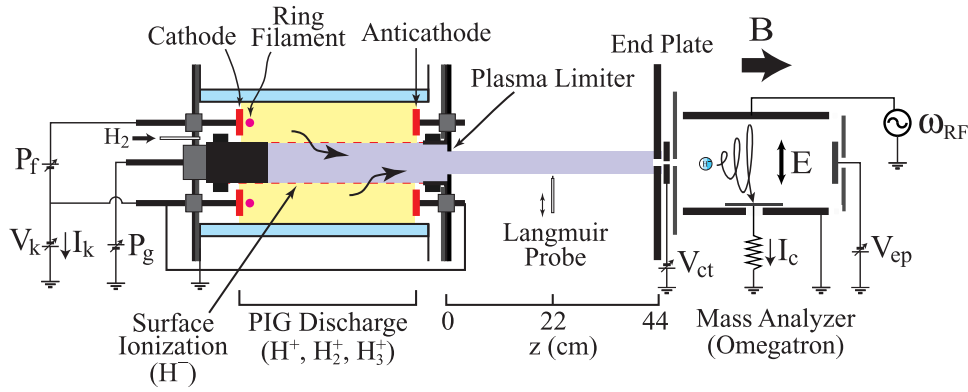


Fig. 1 Schematic diagram of experimental setup. Hydrogen plasma source using catalyst grid consists of a hollow PIG-discharge region and a surface-production part through inward diffusion with magnetic-filter effect.

tion perpendicular to the B -field lines, and the ions entering from the aperture are excited at their various cyclotron resonances, causing their orbital radii to increase. The ion current I_c induced when they strike a collector situated at an off-axis position of the aperture is measured. A spectrum of I_c as a function of the rf frequency $\omega_{RF}/2\pi$, i.e., a mass spectrum, is obtained by slowly sweeping the frequency. The plasma parameters are measured using a Langmuir probe at $z = 22$ cm.

A steady-state hydrogen plasma is generated by the PIG discharge. With the Ni grid, radial profiles of saturation currents and a floating potential of the probe measured at $z = 22$ cm are shown in Fig. 2, where I_+ and I_- denote positive and negative saturation currents of the probe at bias voltages $V_p = -80$ and 80 V, respectively. I_+ is proportional to the positive-ion density n_+ , i.e., the plasma density. I_- is the total electron and negative-ion saturation currents, and its value changes substantially depending on the negative-ion density n_- . The two dashed lines at $|r| = 1.25$ cm denote the inner diameter of the plasma limiter ($\phi 2.5$ cm), which is set at $z = 0$ cm. The plasma produced in the hollow discharge region inwardly diffuses and is supplied downstream ($z > 0$ cm). Therefore, the plasma density is relatively high at $|r| \sim 1$ cm close to the dashed lines. The probe characteristics of the plasma without and with the grid at the radial center ($r = 0$ cm) are measured, not shown here. Without the grid, the electron temperature and the space potential are $T_e \sim 5$ eV and $\phi_s \sim +20$ V, as obtained from the probe characteristic, respectively. Since the temperature is relatively high (> 1 eV), negative ions are not produced by volume production, and the plasma consists only of electrons and positive ions. Then the electron density (the plasma density) of $n_e \sim 3 \times 10^{10}$ cm $^{-3}$ is obtained. The Debye length is about $100 \mu\text{m}$ here, and the grid opening of $77 \mu\text{m}$ is narrower than the Debye

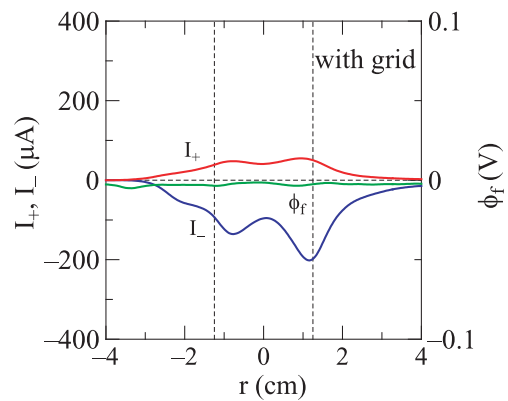


Fig. 2 Radial profiles of saturation currents and floating potential of the probe with the grid at $z = 22$ cm. Inner diameter of plasma limiter is indicated by two dashed lines.

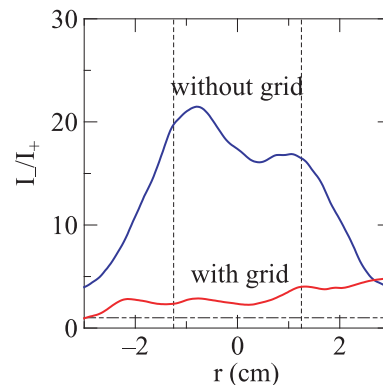


Fig. 3 Radial profiles of the saturation-current ratios without and with the grid.

length. With the grid, the plasma density through the grid decreases substantially. The density is calculated as $n_+ \sim 2 \times 10^9$ cm $^{-3}$ when the positive-ion current is proportional to the density.

Radial profiles of saturation current ratio I_-/I_+ without and with the grid are shown in Fig. 3. The

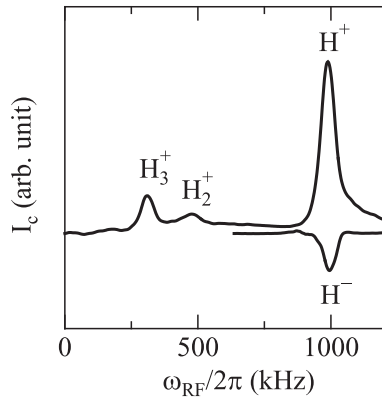


Fig. 4 Typical mass spectrum of omegatron with the grid. Positive and negative peaks denote ion currents of H^+ , H_2^+ , H_3^+ , and H^- .

observed current ratio without the grid is $I_-/I_+ \sim 17$ at $r = 0$ cm. Ideal current ratios without negative ions are calculated as $I_-/I_+ = 0.658\sqrt{m_+/m_-} = 28$ ($H^+ - e^-$ plasma) and 49 ($H_3^+ - e^-$ plasma). The observed current ratio with the grid is $I_-/I_+ \sim 2.4$ at $r = 0$ cm and becomes appreciably low. The negative saturation current is denoted as $I_- = 0.25en_+S((1 - \varepsilon)v_e + \varepsilon v_-)$ from conventional probe theory, where ε is the exchange rate of n_-/n_+ , S is the collector area of the probe (3 mm²), and v_e and v_- are the thermal velocities of electrons and negative ions, respectively. The electron density with the grid cannot be obtained from the probe characteristic, because the exchange rate is unclear. Furthermore, it is difficult to obtain the electron temperature from the probe characteristic at the high exchange rate, because the shielding effect against electric fields is affected by the existence of negative ions. The electron temperature seems to be low because visible emission from the plasma is not observed downstream ($z > 0$ cm). The calculated exchange rate is $\varepsilon = 0.58 - 0.81$ (supposition with $T_- = 0.2$ eV) in $T_e = 1 - 5$ eV. Thus, electrons of about 70 % are changed to negative ions. For the pair-ion plasma generation, all electrons must be changed to negative ions. H^- destruction cross sections [18] are $\sigma \sim 10^{-16}$ cm² ($e^- + H^- \rightarrow H + 2e^-$) and 10^{-13} cm² ($H^+ + H^- \rightarrow 2H$), and mean free paths of H^- are in the order of 10^7 cm and 10^3 cm, respectively, which are much longer than the distance of 22 cm between the source and the probe. Thus, the negative-ion density in $z < 0$ cm seems to be almost the same as that at $z = 22$ cm. The structure in which the plasma diffuses through the grid across the B -field lines is a kind of magnetic filter, and the negative ions produced on the surface are spatially separated from high-energy electrons in the discharge region. In this point, this source differs largely from the conventional negative-ion sources of the converter type [19].

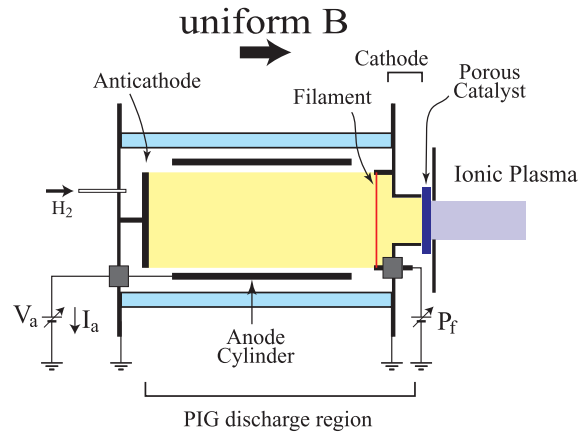


Fig. 5 Schematic drawing of hydrogen plasma source using porous catalyst.

The ion species are analyzed using the omegatron at $B = 65$ mT. Typical mass spectrum with the grid is shown in Fig. 4. The ion cyclotron frequency of H^+ is calculated to be $\omega_c/2\pi = 987$ kHz. Positive and negative peaks at around $\omega_c/2\pi$ in the spectra indicate the existence of H^+ and H^- , respectively. Peaks at the one-half and the one-third frequencies of $\omega_c/2\pi$ indicate the existence of H_2^+ and H_3^+ , respectively. The production of H^+ and H^- is considered to be promoted on the catalyst surface. This production method using catalyst is of advantage for development of negative-ion sources under a cesium-free condition.

3. Penetration-Type Plasma Source

The plasma density in the PIG-discharge region is in the order of 10^{11} cm⁻³. For the diffusion-type plasma source described above, the density decreases one order of magnitude due to diffusion perpendicular to the B -field lines, which is in the case without the grid. Furthermore, the density decreases one order of magnitude due to loss at the grid and is in the order of 10^9 cm⁻³, which is in the case with the grid. The diffusion from the discharge region has a role as a magnetic filter dividing electrons from negative ions spatially. The pair-ion plasma without electrons using fullerene was realized to be generated by ambipolar diffusion in the magnetic filter when negative ions are produced enough a lot. However, electrons also diffuse because the negative-ion production is not enough in the hydrogen plasma. Therefore, it is difficult to eliminate electrons strictly using only the magnetic filter. A penetration-type plasma source without the magnetic filter is developed by using the catalytic reaction. Schematic drawing of the source is shown in Fig. 5.

The hydrogen plasma for supply positive ions to the catalyst surface is generated by the PIG discharge. The cathode plates are set in the both ends neighborhood of a cylindrical anode. The cathode on the side

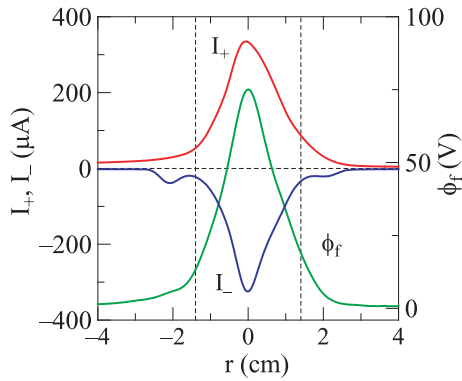


Fig. 6 Radial profiles of saturation currents and floating potential of the probe at $z = 22$ cm.

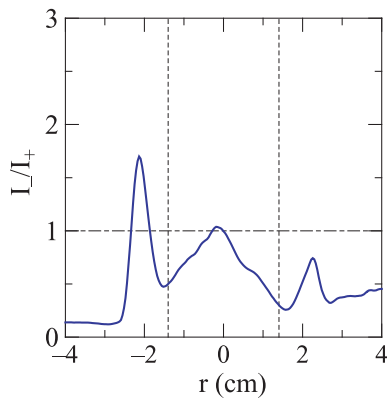


Fig. 7 Radial profile of the saturation-current ratio.

of the plasma source exit is a Ni catalyst and a filament for emitter of thermal electrons is located adjacent. The filament also has the role to heat the catalyst by radiation heat. The catalyst of Ni is a porous body of 48-52 cell/inch, pore size of 0.5 mm, thickness of 2 mm, and specific surface area of $7,500 \text{ m}^2/\text{m}^3$. The catalyst potential becomes a reference potential for the plasma downstream, and is ground here. So the cathodes are grounded and the anode is positively biased, which is different from the diffusion-type source. In normal operation, the anode is typically biased at $V_a \simeq +160 \text{ V}$ (fixed discharge current of $I_a = 2 \text{ A}$). The B field, the gas pressure, and the measurement system are the same as in the diffusion-type source

The porous-catalyst temperature without the discharge ($V_a = 0 \text{ V}$) becomes about $185 \text{ }^\circ\text{C}$ by radiation heat from the filament ($P_f = 16 \text{ A} \times 4 \text{ V}$), and the ions are not observed downstream. The temperature with irradiation of the discharge plasma becomes about $430 \text{ }^\circ\text{C}$, and an ionic plasma with very low electron density is generated downstream. Radial profiles of the saturation currents and the floating potential of the probe at $z = 22 \text{ cm}$ are shown in Fig. 6, where I_+ and I_- is the saturation currents at $V_p = -200$ and 200 V , respectively. The plasma radial profile is almost

Gaussian and the floating potential is $+75 \text{ V}$ at $r = 0 \text{ cm}$. The catalyst is a part of the cathodes, positive ions are accelerated in the sheath formed in front of the cathodes and irrupt to the catalyst. Since the floating potential is relatively high, it is thought that positive ions produced in the discharge region are not terminated completely at the catalyst and the beam ions partially pass through to downstream. Electrons will also pass through partially because of the defective termination. The density is calculated from I_+ at $r = 0 \text{ cm}$ as $n_+ \sim 2 \times 10^{10} \text{ cm}^{-3}$, and the plasma density is one order of magnitude higher than it in the diffusion-type source.

A radial profile of I_-/I_+ is shown in Fig. 7. The observed current ratio is $I_-/I_+ \sim 1.05$ at $r = 0 \text{ cm}$. The plasma generated is an ionic plasma consisting of positive and negative ions with very low density of electrons. There is a region in $I_-/I_+ < 1$ because of the beam-ion interfusion. And electrons will be localized around $|r| \sim 2 \text{ cm}$ outside of the plasma limiter because I_-/I_+ increases here. The localized density increases in proportion to the gas pressure, and so the electrons will diffuse dominantly from the central region to the periphery region by the collision with the neutral particles. In previous works [20], it was observed that negative ions diffuse dominantly to the periphery region and localized due to drift-wave excitation in a negative-ion plasma with relatively low exchange rate. Electrons and negative ions of equal charge tend to separate in the respective region. This phenomenon is qualitatively similar to the electron localization here, though the diffused particle species is different.

4. Discussion

The generation mechanism of the ionic plasma here is considered as follows. The discharge plasma is irradiated to the catalyst surface, and electrons and positive ions are terminated at the surface once. Atomic hydrogen is produced by dissociative adsorption. The atomic hydrogen bonds with the surface material atom and can move along the surface, i.e., surface migration, which is a fundamental phenomenon on catalysts such as Ni and platinum metals. The atomic hydrogen migrates to the backside of the irradiation side along the pore surface of the porous catalyst. Electronic transition occurs between the surface metal and the atoms during the desorption from the surface, and the atomic ions, H^+ and H^- , are consequently produced, i.e., desorption ionization. When both shared electrons transfer to the metal in the desorption, H^+ is produced. On the other hand, when the electrons transfer to the hydrogen, H^- is produced. The details of this process are unclear, but it seems from the experimental results that the desorption ion-

ization is caused. The band structure of the metal surface depending on materials is considered to strongly affect what is most easily produced, H^+ , H^- , or H . Ni is used as the catalyst here, but it is necessary to search the materials for more efficient and balanced ionization of H^+ and H^- . The passage problem of the beam ions and electrons will be overcome by appropriate adjustment of the catalyst thickness.

Acknowledgments

The authors would like to thank Dr. R. Hatakeyama for his encouragement. This work was supported by KAKENHI 18684033, a Grant-in-Aid for Young Scientists (A) from the Ministry of Education, Culture, Sports, Science and Technology, Japan.

- [1] N. Iwamoto, Phys. Rev. E **47**, 604 (1993).
- [2] G. P. Zank and R. G. Greaves, Phys. Rev. E **51**, 6079 (1995).
- [3] H. Schamel and A. Luque, New J. Phys. **7**, 69 (2005).
- [4] B. Eliasson and P. K. Shukla, Phys. Rev. E **71**, 046402 (2005).
- [5] B. Zhao and J. Zheng, Phys. Plasmas **14**, 062106 (2007)
- [6] M. D. Tinkle, R. G. Greaves, and C. M. Surko, Phys. Plasmas **2**, 2880 (1995).
- [7] H. Boehmer, M. Adams, and N. Rynn, Phys. Plasmas **2**, 4369 (1995).
- [8] E. P. Liang, S. C. Wilks, and M. Tabak, Phys. Rev. Lett. **81**, 4887 (1998).
- [9] W. Oohara and R. Hatakeyama, Phys. Rev. Lett. **91**, 205005 (2003).
- [10] W. Oohara, D. Date, and R. Hatakeyama, Phys. Rev. Lett. **95**, 175003 (2005).
- [11] W. Oohara and R. Hatakeyama, Phys. Plasmas **14**, 055704 (2007).
- [12] W. Oohara, Y. Kuwabara, and R. Hatakeyama, Phys. Rev. E **75**, 056403 (2007).
- [13] Y. Takeiri *et al.*, Rev. Sci. Instrum. **70**, 4260 (1999).
- [14] H. Oguri, T. Tomisawa, M. Kinsho, Y. Okamura, and M. Mizumoto, Rev. Sci. Instrum. **71**, 975 (2000).
- [15] M. Bacal, Nucl. Fusion **46**, S250 (2006).
- [16] O. Fukumasa and S. Mori, Nucl. Fusion **46**, S287 (2006).
- [17] H. Somer, H. A. Thomas, and J. A. Hipple, Phys. Rev. **82**, 697 (1951)
- [18] K. Prelec and Th. Sluyters, Rev. Sci. Instrum. **44**, 1451 (1973)
- [19] K. N. Leung and K. W. Ehlers, J. Appl. Phys. **52**, 3905 (1981)
- [20] W. Oohara and R. Hatakeyama, Trans. Fusion Sci. Tech. **43**, 216 (2003).